

BASIC AND APPLIED RESEARCH RELATED TO
THE TECHNOLOGY OF SPACE ENERGY
CONVERSION SYSTEMS

Semi-Annual Report
February 8, 1988 - August 8, 1988

NASA Grant NAG 1-327

Principal Investigators

A. Hertzberg *A. Hertzberg*

A.T. Mattick *John I. Mattick*

A.P. Bruckner *Adam Bruckner*

BASIC AND APPLIED RESEARCH RELATED TO THE TECHNOLOGY
OF SPACE ENERGY CONVERSION SYSTEMS

Semi-Annual Report
February 8, 1988 - August 8, 1988

NASA Grant NAG 1-327
University of Washington
Seattle, WA 98195

I. LIQUID DROPLET RADIATOR (LDR)

The first six months' research effort on the LDR has focussed on experimental and theoretical studies of radiation by an LDR droplet cloud. Improvements in the diagnostics for our radiation facility have been made which have enabled an accurate experimental test of theoretical predictions of LDR radiation over a wide range of optical depths, using a cloud of Dow 704 silicone oil droplets. In conjunction with these measurements we have made an analysis of the evolution of the cylindrical droplet cloud generated by our 2300-hole orifice plate. This analysis indicates that a considerable degree of agglomeration of droplets occurs over the first meter of travel. Our theoretical studies have centered on development of an efficient means of computing the angular scattering distribution from droplets in an LDR droplet cloud, so that a parameter study can be carried out for LDR radiative performance vs fluid optical properties and cloud geometry.

Droplet Cloud Radiation Experiments

Our radiation measurement facility was used to determine the normal emissivity of a cylindrical cloud of 2300 droplet streams (Dow 705 fluid), as a function of the diametrical optical depth of the cloud. Previous experimental measurements of droplet cloud emissivity carried out with earlier generations of this facility were not sufficiently accurate to provide a definitive test of our theory of LDR radiation

transfer. Although the dependence of cloud emissivity on optical depth was found to correspond roughly with theory, an anomalously low value of droplet emittance was indicated. The principal sources of error in the previous measurements were optical depth fluctuations (remedied by the acoustical baffles), and the uncertainty in the background radiation contribution to the droplet radiation signal.

This year we have improved the radiation diagnostics by incorporation a cooled radiation baffle to precisely define the background signal during our experiments. The detector module is actively cooled by water to maintain a constant temperature both for the detector and for the walls of the baffle. The baffle, coated with a high emissivity paint, absorbs any radiation lying outside a precisely defined viewing cone (5.3° half angle). The experimental approach is designed to eliminate the need for absolute power measurements. During an experimental run, a flow of droplets is maintained for 1-2 hours to achieve thermal equilibrium of components in the transit chamber and to fully outgas the heated silicone oil. During this time the cooled shutter for the detector is closed. The shutter is then opened and the droplet radiation signal is recorded for a period of several seconds. The droplet flow is then stopped, and the decrease in radiation signal is recorded. During this process, a background surface (behind the droplets and intercepting the full viewing angle of the detector) is maintained at constant temperature. Only the difference in power with droplet streams on and off is required to determine the emissivity of the droplet cloud.

We have been able to measure the normal cloud emissivity over an optical depth range of 0.5 to 3.5 by making use of the decrease in optical depth with transit distance due to stream divergence and droplet agglomeration (see below). Fig. 1 shows the results of our radiation measurements. Each triangle represents an averaged set of data for normal cloud emissivity for several experimental runs, and the solid lines are theoretical predictions of normal emissivity for droplet emittances

of 0.8, 0.9 and 1.0. Based on spectral absorption and reflection measurements, the emittance of 350- micron droplets of Dow 704 is predicted to be 0.9 ± 0.02 . It is evident that our experimental results are in good agreement with theory over the range of optical depths 0.6 to 3.3.

Evolution of Droplet Cloud

The decrease of optical depth of the droplet cloud with transit distance was used to avail in the above-described radiation measurements, but this decrease also represents a potential difficulty for implementation of effective LDR systems in space, which typically would require transit distances of 10's of meters. The principal causes for decrease in optical depth in our experiment include 1) Divergence of droplet streams; 2) Agglomeration of droplets; and 3) Gravitational acceleration. The third effect would, of course, be absent in a space-based LDR, but the first two effects may be important. These two effects are related, since agglomeration results from collisions of non-parallel droplet streams.

We have conducted an analysis of this optical depth decrease in conjunction with our radiation experiments in order to determine the degree of decrease due to directly to stream divergence and that due to agglomeration. Droplet streams emerge from the generator with a range of angles from vertical, due partly to outward bowing of the orifice plate from the applied fluid pressure in the plenum, and partly to imperfections in the shape and alignment of the individual orifices. The random divergence due to orifice imperfections leads to droplet collisions and agglomeration, which decreases the optical depth of the cloud. The variation of optical depth with transit distance can be expressed as:

$$\tau/\tau_0 = (\tau_0/r) / (1 + 2\phi x/D_0) / \sqrt{1 + \rho g x/P}$$

where r_0 is the droplet radius at a reference station 13-cm from the generator, r is the radius at a test station a distance $x = 85$ cm downstream of this reference station, D_0 is the cloud radius at the reference, ϕ is the divergence angle, $\rho = 1.0 \text{ gm/cm}^3$ is the liquid density, and P is the plenum pressure. Pressures of 7.0 psi and 8.5 psi were used for this analysis. The first term results from agglomeration, the second from divergence, and the third from gravitational acceleration.

Analysis of photographs of the droplet cloud indicated a spreading angle ϕ of 0.044 ± 0.02 rad at $P=7$ psi, and 0.056 ± 0.02 rad at 8.5 psi. The ratio of optical depths between reference and test stations was 3.05 ± 0.2 at both pressures, over a wide range of driving frequencies. From this data, we observe that $r/r_0 = 1.38$ at 7 psi and $r/r_0 = 1.21$ at 8.5 psi. The fraction of droplets remaining at the test station is $(r_0/r)^3$, or 0.38 at a pressure $P = 7.0$ psi, and 0.56 at 8.5 psi. This is confirmed qualitatively by photographs, and the decrease in agglomeration with increasing pressure is reasonable, since the higher stream divergence reduces the chance of droplet collisions.

These results indicate that agglomeration and stream divergence are an important design considerations for the LDR. Decrease of optical depth with distance will reduce the sheet emissivity and power/mass of the droplet sheet, and divergence, specifically, will require large (and heavy) droplet collectors to prevent fluid loss. Wider spacing of orifices (and thicker droplet sheets) may be required to minimize agglomeration, and stiffeners in the orifice plate may be required to minimize divergence due to plate bowing.

Theoretical Analysis of Droplet Cloud Radiation

We have concentrated on developing efficient codes for predicting droplet sheet emissivity (planar geometry), which include wave effects on scattering and absorption cross-sections as well as non-isotropic scattering (Mie scattering). These codes are based on analysis carried out in the previous grant period. Our chief accomplishment thus far in the grant period is the development of an efficient algorithm for approximating the angular distribution of Mie scattering with a Legendre polynomial series. This approximation must only closely match the actual angular distribution for scattering angles $> 45^\circ$, since forward scattering has little or no effect on the emissivity of a droplet sheet. We have tested our algorithm for a wide range of droplet diameters, wavelengths and fluid optical properties, and have found it sufficiently accurate for droplet sheet computations. Typically terms only to 2nd order are needed for accuracies in sheet emissivity of 0.001, although in exceptional cases (small index of refraction, large absorption, and size parameters from 5 to 50) 3 terms are needed to achieve an accuracy of 0.001. We are now coding a routine to compute the thermal (rather than spectral) emissivity of a droplet sheet, and will use this code to carry out a parameter study of LDR sheet thermal emissivity vs fluid properties, droplet size, temperature, and cloud dimensions.

II. LIQUID DROPLET HEAT EXCHANGER (LDHX)

During the past six months the modifications to the LDHX experiment facility for test on NASA's KC-135 reduced-gravity aircraft were completed and the flight tests took place June 21-23 at Ellington Field in Houston, TX. The experiments focused on the two-phase flow dynamics, thus heat transfer measurements were not performed on this flight. Quantitative and qualitative measurements of the flow process were carried out to better understand the feasibility of this concept, and its potential for improving upon present space-based heat exchanger designs.

The LDHX reduced gravity flight test was designed to model (to first order) the zero-gravity behavior of the two-phase flow process envisioned within an operational LDHX. Quantitative and qualitative measurements of the flow process were carried out to better understand the feasibility of this concept, and its potential for improving upon present space-based heat exchanger designs. Specific test objectives for the flight tests were:

- 1) To determine the effectiveness of the zero-g phase separation scheme following the gas/droplet interaction. The collected liquid from the skimmers would be compared with any liquid carried over and collected in the gas exhaust phase separator. These results would be compared with the baseline one-g laboratory tests.
- 2) To capture the qualitative nature of the two-phase flow interaction and phase separation scheme on video tape and still photographs.
- 3) To measure the static and total pressure profiles across the vortex chamber for a variety of gas and liquid flow rates, for comparison with baseline measurements made in the laboratory.
- 4) To determine if secondary flow effects or other problems become dominant enough in zero-g to interfere with the expected two-phase flow interaction and phase separation scheme.

5) To make recommendations regarding future directions for LDHX development, based upon the results of the above objectives.

Experimental Apparatus

A schematic of the flight experiment is shown in Fig. 2. The gas flow was provided by four compressed air bottles, each 1.54 cu ft in volume, and holding 2200-2250 psig when full. The compressed air bottles provided pressure for the water supply, in addition to being the source of the gas phase for the experiment. The air flow was directed from the bottles into a stainless steel manifold, through a master shut-off valve, then to either 1) the vortex chamber or 2) the hydropneumatic tank.

Air flow into the vortex chamber first passed through a two stage regulator, a relief valve (set pressure = 125 psi), a manual flow control valve, a computer controlled solenoid valve, a sonic orifice (to meter the flow rate into the vortex chamber) and then to a flow splitter which distributed the flow equally around the periphery of the vortex chamber. Once injected into the chamber, the flow spiraled to the core, and exited out the bottom into the air exhaust phase separator (also referred to as the core separator) through a manual backpressure control valve, and to the atmosphere. The two-stage regulator in this flow path was set to deliver a flow pressure of 100 psia, which corresponds to approximately 87.7 psig with the aircraft atmosphere at 5000 ft (12.3 psia). With no flow, the regulator setting was a maximum of 116 psi. The three sonic orifices available provided a range of air flow rates from 11 to 30 gm/sec. The air exhaust phase separator was present to remove any entrained liquid before exhausting the air to the atmosphere.

Air flow into the hydropneumatic tank first passed through a single stage regulator (designed for dead-ended service) and a relief valve (set pressure = 90 psi) before being applied to one side of the tank. The regulator was set to a maximum delivery pressure of 80 psig. The tank is separated into air and water chambers by a

flexible rubber diaphragm. Water was driven into the experiment at the rate of 9.5 to 12.6 gm/sec. The diaphragm adjusted its position to remain in contact with the water as the fluid volume dropped during testing. Water flowed from the tank through a 60 micron filter, a manual flow control valve, a computer controlled solenoid valve, a metering valve and flow meter (to set the flow rate into the chamber), a 15 micron filter, and into a water manifold which distributed the water to 36 droplet tubes at the core of the vortex chamber. The water was removed from the chamber by the skimmers, and passed through the skimmer phase separator, which removed any air skimmed with the water. At the end of each run, computer controlled solenoid dump valves opened to drain the phase separators into lower level holding tanks as the aircraft went through positive-g in preparation for the next parabola.

A planview schematic of the experiment layout installed on the KC-135 is shown in Fig. 3. The experiment support structure held the vortex chamber, phase separators and liquid holding tanks. The equipment rack housed pressure gauges, manual and solenoid valves, filters and flow meter, a data acquisition system, the sonic orifice turntable, a video tape recorder, solid state relays and power supplies. The hydropneumatic tank was caged by a third structure. Each of the three structures was mounted on an aluminum baseplate, which mounted to the aircraft via bolts located on a 20 in. grid, matching the tie-down grid on the floor of the aircraft. The compressed air bottles were mounted to a rack supplied by the Reduced Gravity Office.

Experiment Procedure

Two test personnel took part in experiment operations and data acquisition. One was stationed at the computer, and controlled run sequencing, monitored flow parameters, started data acquisition during total pressure runs, reviewed sensor performance as it was plotted on the monitor immediately after each run, and

coordinated data storage to disk following each run. A second operator, stationed at the vortex chamber, was responsible for manipulating the total pressure probe during total pressure data acquisition, adjusting skimmer heights to match liquid film thickness on the vortex sidewall, monitoring air exhaust and skimmer separator performance, and checking liquid dump tank quantities between parabolas. During static pressure runs, this operator was responsible for photographic data acquisition, operating either a 35mm still camera or a video camera and video tape recorder, together with a strobe light for flow illumination. This operator was also responsible for sonic orifice selection prior to a set of parabolas, and air and water regulator adjustments.

The video camera was mounted on a support securing the camera in any desired position. The video recorder was in the record mode for the duration of the flight, allowing hands-off video data acquisition during total pressure runs. The strobe light was secured using velcro to allow unattended operation of it as well.

As the aircraft entered a parabola, the computer operator started a data collection run on the computer. The computer commanded the air and water solenoid valves to open, and began sampling the pressure and temperature transducers. During static pressure runs, the second operator photographed predetermined locations within the chamber. During total pressure runs, the second operator coordinated with the computer operator to position the total pressure probe for data collection. When the computer completed measurements (approximately 15 seconds in duration), it closed the water and air solenoid valves, and opened the dump valves to drain the phase separators into their respective holding tanks.

Preliminary Test Results

1) Skimmer efficiency in zero-g as compared to one-g (baseline lab tests) was found to be significantly higher at all gas and water flows investigated, approaching 100% in the runs at the higher gas flow rates.

2) In general, the two-phase flow interaction in zero-g (away from the sidewall) was similar to that in one-g. The secondary separators proved effective in capturing any entrained liquid before exhausting the air into the cabin.

3) Static and total pressure profiles were measured for various gas and water flow rates, and found to be quite similar to corresponding ground-based measurements. The static pressure profiles were more easily obtained (one complete profile per parabola) than the total pressure profiles (one port location per parabola), hence the static pressure profiles that will be plotted from these runs will be better characterized and more complete than the total pressure profiles.

4) No secondary flow effects or other problems were observed which seriously interfered with the expected two-phase flow interaction and phase separation scheme. Liquid reaching the sidewall upstream of the skimmers was fully collected by the skimmers, in contrast to one-g flow, in which liquid runoff caused overloading of the skimmer at the base of the sidewall. However, liquid encountering the sidewall, in the 2 inch section downstream of each skimmer but upstream of each air injection port, was adversely affected by surface tension. As the liquid film reached the edge of each air injection port, a portion of the film was pulled away from the wall (in the form of large drops) by the incoming air flow. The remaining film spread vertically over the height of the sidewall until encountering the endplates. Here the liquid clung to the corners created by the sidewall and endplate surfaces. The accumulated liquid formed streams, which were pulled away from the corners by the incoming air flow. These streams were pulled along the top and bottom endplates to the core of the chamber, and exited with the air exhaust.

5) A piezoelectric driver was successfully used to generate uniform droplets streams. No significant changes in the droplet generation process were observed from one-g to zero-g. The uniform nature of the driven droplet streams was best visualized at the lowest air mass flow rate, where turbulence was at a minimum. With increased air flow rate, the streams became less coherent. The high air flow rate produced a homogeneous cloud of droplets with no discernible individual droplet streams.

Conclusions

The recent zero-g test flights of the LDHX experiment represent the successful culmination of the second phase of LDHX research. Considerable data on the zero-g behavior of the device was obtained; much of this is in the process of being analyzed and will be reported in greater detail at a later date. In general, no problems were discovered in zero-g which would act as impediments to further development of the concept. As expected, skimmer efficiency increased significantly in zero-g, compared to one-g. The two-phase interaction in the vortex chamber appeared to be similar to that in one-g, and no secondary flow problems were encountered. The effects of surface tension in zero-g were found to cause some of the liquid film at the cylindrical chamber walls to re-enter the swirling gas flow, however, these effects can be eliminated through a slight change in wall geometry and by relocating the liquid skimmers closer to the gas injection ports.

EXPERIMENTAL MEASUREMENT OF CLOUD EMISSIVITY

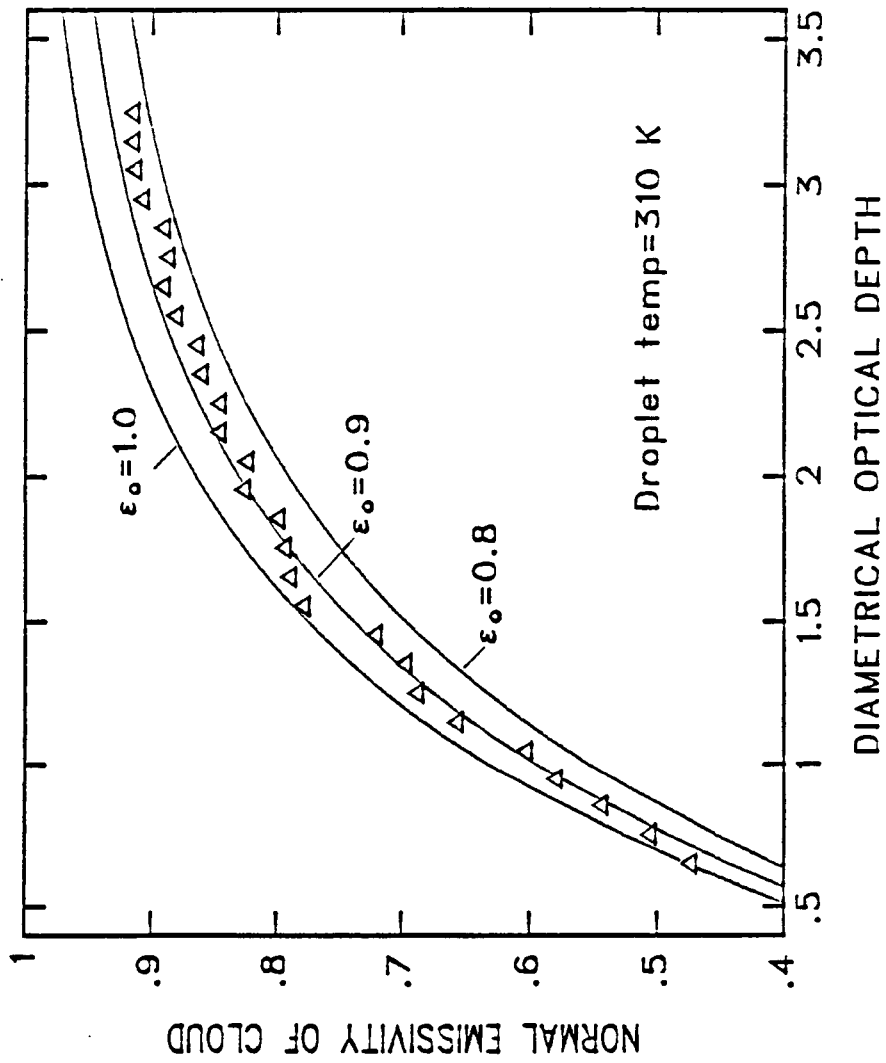


Figure 1.

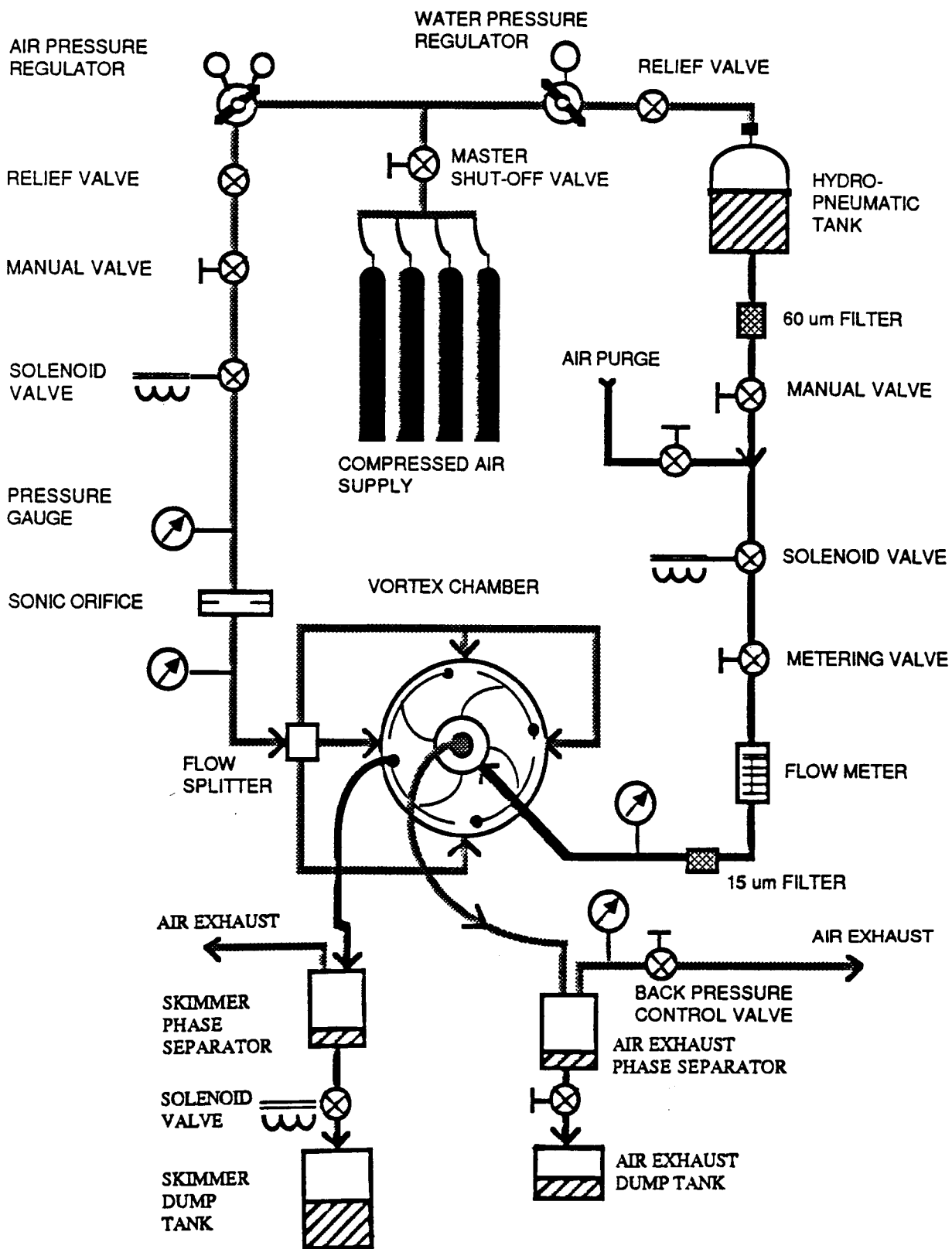


Fig. 2 LDHX Flight Experiment Schematic

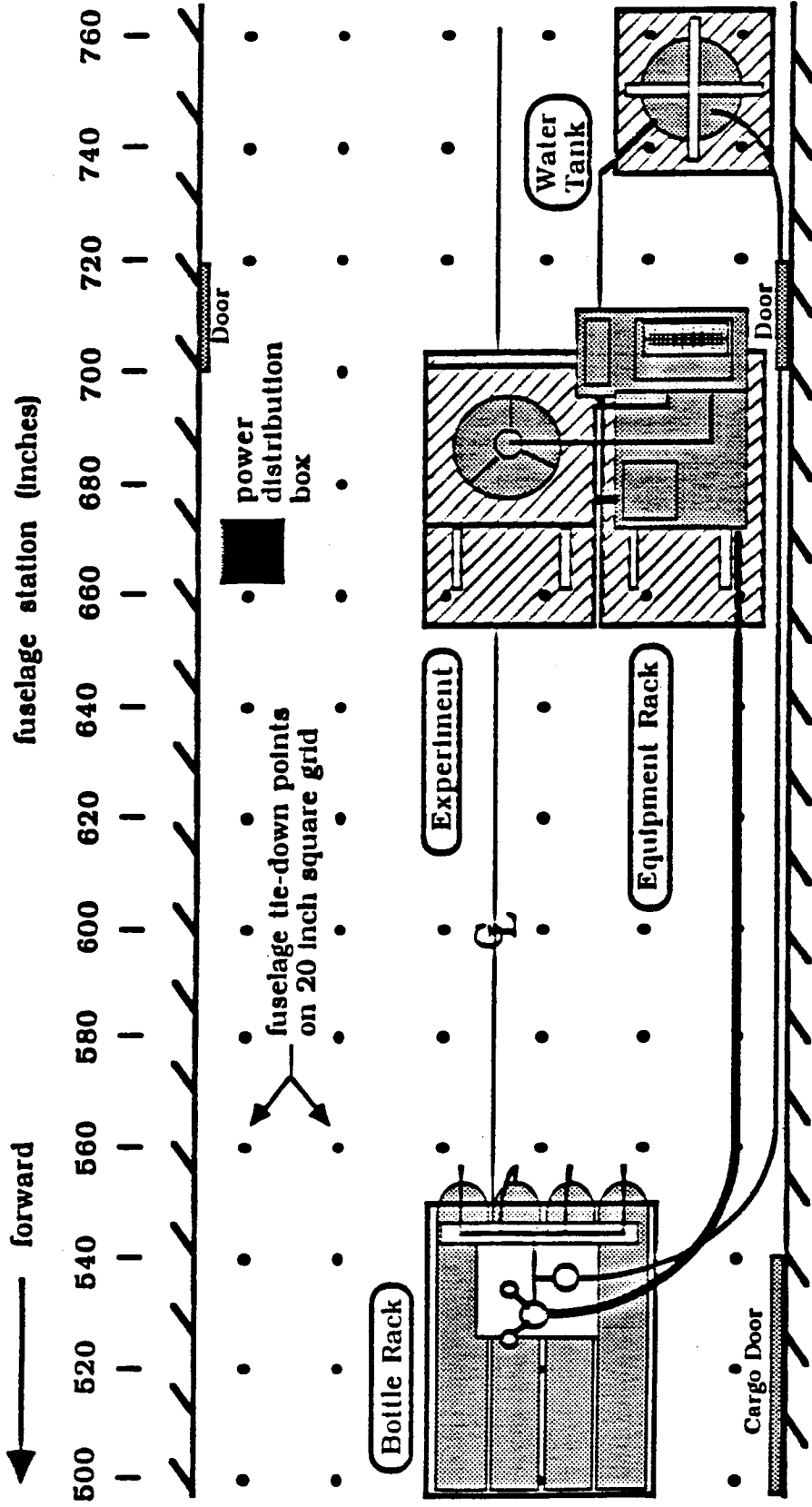


Fig. 3 Planview of LDHX Layout on KC-135 Aircraft